NASA TECHNICAL MEMORANDUM

UB
NASA TM X-1712

VERTICAL-TAIL LOADS AND CONTROL-SURFACE HINGE-MOMENT MEASUREMENTS ON THE M2-F2 LIFTING BODY DURING INITIAL SUBSONIC FLIGHT TESTS

by Jerald M. Jenkins, Ming H. Tang, and George P. E. Pearson

Flight Research Center
Edwards, Calif.

NATIONAL AERONAUTICS AND SPACE ADMINISTRATION • WASHINGTON, D. C. • DECEMBER 1968

NASA TM X-1712

VERTICAL-TAIL LOADS AND CONTROL-SURFACE HINGE-MOMENT MEASUREMENTS ON THE M2-F2 LIFTING BODY DURING INITIAL SUBSONIC FLIGHT TESTS

By Jerald M. Jenkins, Ming H. Tang,
and George P. E. Pearson

Flight Research Center
Edwards, Calif.

NATIONAL AERONAUTICS AND SPACE ADMINISTRATION

VERTICAL-TAIL LOADS AND CONTROL-SURFACE HINGE-MOMENT MEASUREMENTS ON THE M2-F2 LIFTING BODY DURING INITIAL SUBSONIC FLIGHT TESTS*

By Jerald M. Jenkins, Ming H. Tang,
and George P. E. Pearson
Flight Research Center

SUMMARY

Subsonic aerodynamic load characteristics are presented for the right vertical tail and the control surfaces of the M2-F2 lifting-body vehicle. The effects of vehicle attitude and control-surface deflection on the vertical-tail loads are determined. Coefficients defining the effects of angle of attack, angle of sideslip, upper-flap deflection, and rudder deflection on flight-measured vertical-tail loads are presented in terms of linear equations. Portions of two maneuver time histories are included to illustrate the magnitude of each of these effects. The effects of angle of attack and control-surface deflection on the flight-measured rudder, upper-flap, and lower-flap hinge moments are discussed. The measured loads data are presented in aerodynamic-coefficient form. Large vertical-tail loads were measured during flight tests. Flight-measured control-surface hinge-moment data are compared with wind-tunnel data obtained from full-scale vehicle tests.

INTRODUCTION

The increasing number and scope of manned space missions has led to a need for advanced reentry/recovery concepts. Vehicles having improved maneuvering capabilities provide distinct advantages over present recovery capabilities. The lifting reentry vehicle has increased maneuvering capability and has thus been studied (refs. 1 to 4) for manned reentry.

One of the more important areas of investigation with this type of vehicle is low-speed flight characteristics, inasmuch as virtually no flight-test information is available for the wingless, short-fuselage, lifting-body configuration. Accordingly, a series of flight tests was performed with one lifting-body configuration, designated the M2-F2. The flight-determined lift and drag characteristics and stability and control characteristics are presented in references 5 and 6, respectively. The M2-F2 flight vehicle was also tested in the 40- by 80-Foot Wind Tunnel at the NASA Ames Research Center. Results of these tests are reported in reference 7. The low-speed aerodynamic-loads data acquired from full-scale flight tests of the M2-F2 are presented in this report. A knowledge of the magnitude of these aerodynamic loads is important to designers of lifting-body vehicles, particularly since the M2-F2 is a unique configuration.

---

*Title, Unclassified.

Strain-gage instrumentation was used to measure vertical-tail loads and control-surface hinge moments during the M2-F2 research flights. The flight data were obtained during initial unpowered glide flights; hence, the data are limited to subsonic Mach numbers from approximately 0.4 to 0.6.

SYMBOLS

B_t vertical-tail bending moment, in-lb (m-N)

b_t reference span of the vertical tail, 2.70 ft (0.823 m)

C_B vertical-tail bending-moment coefficient, $\frac{B_t}{qS_t b_t}$

C_{B_0} vertical-tail bending-moment coefficient at α, β, δ_r, $\delta_u = 0°$

C_{B_α} change in vertical-tail bending-moment coefficient with angle of attack, $\frac{\partial C_B}{\partial \alpha}$, per deg

C_{B_β} change in vertical-tail bending-moment coefficient with angle of sideslip, $\frac{\partial C_B}{\partial \beta}$, per deg

$C_{B_{\delta_r}}$ change in vertical-tail bending-moment coefficient with rudder deflection, $\frac{\partial C_B}{\partial \delta_r}$, per deg

$C_{B_{\delta_u}}$ change in vertical-tail bending-moment coefficient with upper flap deflection, $\frac{\partial C_B}{\partial \delta_u}$, per deg

C_{h_l} lower-flap hinge-moment coefficient, $\frac{H_l}{qS_l \bar{c}_l}$

C_{h_r} rudder hinge-moment coefficient, $\frac{H_r}{qS_r \bar{c}_r}$

C_{h_u} upper-flap hinge-moment coefficient, $\frac{H_u}{qS_u \bar{c}_u}$

C_y vertical-tail normal-force coefficient, $\frac{V_t}{qS_t}$

C_{y_0}	vertical-tail normal-force coefficient at α, β, δ_r, $\delta_u = 0°$
C_{y_α}	change in vertical-tail normal-force coefficient with angle of attack, $\frac{\partial C_y}{\partial \alpha}$, per deg
C_{y_β}	change in vertical-tail normal-force coefficient with angle of sideslip, $\frac{\partial C_y}{\partial \beta}$, per deg
$C_{y_{\delta_r}}$	change in vertical-tail normal-force coefficient with rudder deflection, $\frac{\partial C_y}{\partial \delta_r}$, per deg
$C_{y_{\delta_u}}$	change in vertical-tail normal-force coefficient with upper-flap deflection, $\frac{\partial C_y}{\partial \delta_u}$, per deg
$\bar{c}$	average chord, ft (m)
H	hinge moment, in.-lb (m-N)
M	free-stream Mach number
q	free-stream dynamic pressure, lb/ft^2 (N/m^2)
S	surface area, ft^2 (m^2)
t	time, sec
V_t	vertical-tail shear, lb (N)
X, Y, Z	vehicle reference axes
Z_{cp}	vertical-tail spanwise center-of-pressure location, fraction of reference vertical-tail span, $\frac{C_B}{C_y}$
α	vehicle angle of attack, deg
β	vehicle angle of sideslip, deg
δ	control-surface deflection, deg

Subscripts:

l	lower flap

r	rudder
t	vertical tail
u	upper flap

DESCRIPTION OF THE M2-F2 AIRCRAFT

The M2-F2 research aircraft is shown in figures 1(a) and 1(b). The aircraft is basically half of a 26° cone with a rounded nose, faired afterbody, twin vertical tails, and five control surfaces. A more detailed description and discussion of the M2-F2 is presented in reference 6. A three-view drawing of the vehicle is shown in figure 2. An additional drawing is presented in figure 3 to illustrate the sign conventions used for aircraft parameters pertinent to this report. Physical characteristics of the M2-F2 aircraft are listed in table I.

INSTRUMENTATION

Strain-Gage Installation and Calibration

The vertical tail of the M2-F2 is a structure of very low aspect ratio with numerous spars to transmit aerodynamic loads (fig. 4). Twenty-one strain-gage bridges are installed at various positions along the root of the vertical tail. A large number of bridges were installed since the short spars and thin-skin construction do not provide a structural arrangement that can be calibrated easily.

The structure was calibrated by using a conventional point-by-point loading procedure (ref. 8). The responses of the bridges were recorded on a pulse-code-modulation (PCM) data-acquisition system during the calibration. Loads were applied at 35 load points on the surface of the structure.

The results of the loads calibrations revealed that shear bridges in the forward area of the structure responded only to the load points on the spar to which the individual bridge was mounted. The bridges in the rear part of the structure responded more uniformly; however, these bridges did not respond to load points in the forward part of the structure. These response characteristics eliminated the possibility of using a smaller number of bridges to formulate a conventional load equation. However, a single load equation could be used to express the total applied shear in the section of the tail from the trailing edge to the second spar forward of the rudder hinge line. In the area forward of this section, loads could be obtained only by measuring the load on each spar. Three spars in this area were instrumented.

Flight loads were obtained in the forward section of the vertical tail by measuring the root shear on the three spars and dividing this shear by the respective panel areas to obtain an average panel pressure. The average panel pressures were then plotted against the chord, and a line was faired through these points. The resulting faired pressure line was integrated over the appropriate area, and a total shear was obtained

for the forward section. This shear and the shear obtained for the rear section were then summed to obtain the total shear acting on the vertical tail.

The bending moment was obtained by using a standard load equation. A large number of bridge combinations were investigated, and the most accurate load equations were selected. An analysis of the influence coefficients obtained from the loads calibration revealed that (1) scatter existed in bridge outputs when the influence coefficients were examined on a span and a chord basis and (2) outputs were very low from all bridges for loads at several load points. The combination of these factors made it difficult to obtain accurate best-fit coefficients for the loads equations.

The control-surface hinge-moment instrumentation consisted of strain gages on the actuator mechanisms of the various control surfaces. The control surfaces were calibrated by loading in place on the aircraft and by recording the outputs on a PCM system. No difficulties were experienced in obtaining linear calibrations; however, low strain-gage-bridge outputs due to low load levels occurred during flight tests, which resulted in some scatter in the flight data.

Estimated Errors

Estimates were made of the errors in each of the parameters pertinent to the presentation of the loads data. The estimates include sensor errors, calibration errors, and data-reduction errors. The magnitudes of the estimated errors of the pertinent aircraft and load parameters were:

α, deg	±0.7
β, deg	±0.3
q, lb/ft^2 (N/m^2)	±1.80 (±86.2)
M	±0.01
δ_u, deg	±0.6
δ_l, deg	±0.4
δ_r, deg	±0.3
V_t, lb (N)	±400 (±1780)
B_t, in.-lb (m-N)	±4000 (±452)
H_u, in.-lb (m-N)	±300 (±33.9)
H_l, in.-lb (m-N)	±150 (±17.0)
H_r, in.-lb (m-N)	±250 (±28.3)

DATA REDUCTION

Flight loads measurements were made for the following parameters: right vertical-tail root shear, right vertical-tail root bending moment, upper-flap hinge moment,

rudder hinge moment, and lower-flap hinge moment. All rudder deflections and hinge moments used in this analysis refer to right rudder only.

In order to maintain sufficiently large strain-gage outputs, minimum acceptable levels of dynamic pressure were established to assure that the flight load levels of data analyzed were large enough to provide acceptable accuracy. Vertical-tail-loads data acquired at dynamic pressures less than 225 lb/ft^2 (10,773 N/m^2) were not analyzed. It was similarly determined that accurate data could be obtained from the control-surface hinge-moment instrumentation only when data obtained at a dynamic pressure in excess of 200 lb/ft^2 (9576 N/m^2) were analyzed.

The flight loads data are presented in aerodynamic-coefficient form. The control-surface hinge moments are referenced to their respective hinge lines. The vertical-tail data are referenced to the aircraft horizontal reference line, which is 2.70 feet (0.823 meter) below the tip of the vertical tail.

Vertical Tail

The vertical-tail normal-force coefficient and bending-moment coefficient are defined, respectively, by the following equations:

$$C_y = \frac{V_t}{qS_t} \tag{1}$$

$$C_B = \frac{B_t}{qS_t b_t} \tag{2}$$

Aircraft attitude and the proximity of the control surfaces provide four parameters that affect the magnitude of the vertical-tail loads on a lifting-body vehicle such as the M2-F2. These four contributing parameters are angle of attack, angle of sideslip, upper-flap deflection, and rudder deflection. A fifth parameter, a nonvarying coefficient, is also present as a result of the 3° toe-in of the vertical tail and the unusual flow conditions on a vehicle of this shape. The total aerodynamic-load coefficient may be expressed as the sum of the five components. For the normal-force coefficient, the components are

$$C_y = C_{y_0} + \frac{\partial C_y}{\partial \alpha}\alpha + \frac{\partial C_y}{\partial \beta}\beta + \frac{\partial C_y}{\partial \delta_u}\delta_u - \frac{\partial C_y}{\partial \delta_r}\delta_r \tag{3}$$

For the bending-moment coefficients, the components are

$$C_B = C_{B_0} + \frac{\partial C_B}{\partial \alpha}\alpha + \frac{\partial C_B}{\partial \beta}\beta + \frac{\partial C_B}{\partial \delta_u}\delta_u - \frac{\partial C_B}{\partial \delta_r}\delta_r \tag{4}$$

For simplicity, the flight data were analyzed by assuming the preceding derivatives to be constant coefficients (i.e., linear functions) within the scope of the analysis. On

the basis of this assumption, equations (3) and (4) may be expressed as

$$C_y = C_{y_0} + C_{y_\alpha}\alpha + C_{y_\beta}\beta + C_{y_{\delta_u}}\delta_u - C_{y_{\delta_r}}\delta_r \tag{5}$$

where

$$C_{y_\alpha} = \frac{\partial C_y}{\partial \alpha}, \quad C_{y_\beta} = \frac{\partial C_y}{\partial \beta}, \quad C_{y_{\delta_u}} = \frac{\partial C_y}{\partial \delta_u}, \quad C_{y_{\delta_r}} = \frac{\partial C_y}{\partial \delta_r}$$

and

$$C_B = C_{B_0} + C_{B_\alpha}\alpha + C_{B_\beta}\beta + C_{B_{\delta_u}}\delta_u - C_{B_{\delta_r}}\delta_r \tag{6}$$

where

$$C_{B_\alpha} = \frac{\partial C_B}{\partial \alpha}, \quad C_{B_\beta} = \frac{\partial C_B}{\partial \beta}, \quad C_{B_{\delta_u}} = \frac{\partial C_B}{\partial \delta_u}, \quad C_{B_{\delta_r}} = \frac{\partial C_B}{\partial \delta_r}$$

The analysis of the vertical-tail-loads data was dependent upon the successful evaluation of the five coefficients in equations (5) and (6). The following procedure was used in the analysis:

1. A large number of flight conditions were selected for analysis in order to provide a large range of aircraft attitude and control-surface deflections.

2. The total shear (or bending) load was calculated from flight data and reduced to coefficient form, i.e., C_y (or C_B).

3. The force-coefficient data along with the corresponding values of angle of attack, angle of sideslip, upper-flap deflection, and rudder deflection were programed for a computer which solved for the coefficients by using the least-squares technique.

4. The probable error of the coefficients was determined.

Control-Surface Hinge Moments

The control-surface hinge moments are also presented in aerodynamic-coefficient form. The coefficients for the upper flap, lower flap, and rudder are defined, respectively, as

$$C_{h_u} = \frac{H_u}{qS_u\bar{c}_u} \tag{7}$$

$$C_{h_l} = \frac{H_l}{qS_l\bar{c}_l} \tag{8}$$

$$C_{h_r} = \frac{H_r}{qS_r\bar{c}_r} \tag{9}$$

The reduction of hinge-moment data was straightforward, since responses from single strain-gage bridges were used for each surface. The bridge outputs were directly proportional to hinge-moment values; thus, the bridge output was measured during flight and the corresponding hinge-moment value was calculated.

FLIGHT-TEST PROCEDURE

Research flights of the M2-F2 aircraft began with an air launch from a B-52 carrier aircraft at an altitude of approximately 45,000 feet (13,716 meters). The glide-flight test maneuvers were performed, and the aircraft was landed on a dry lakebed at Edwards Air Force Base, Calif. The data presented in this report were obtained during initial glide flights; therefore, only subsonic data are available. The data were obtained at free-stream dynamic pressures from 200 lb/ft^2 (9576 N/m^2) to 360 lb/ft^2 (17,200 N/m^2) and at Mach numbers from approximately 0.4 to 0.6.

RESULTS AND DISCUSSION

Vertical-Tail Loads

Two maneuvers, from flights M-10 and M-16* were used to analyze vertical-tail-loads data. The values obtained for the 10 coefficients in equations (5) and (6) are presented in table II for the maneuvers. The general flight conditions and the probable errors of the coefficients are also presented. Equations (10) to (13) were obtained from this analysis. For flight M-10

$$C_y = 0.6009 + 0.0221\alpha + 0.0324\beta + 0.0038\delta_u - 0.0109\delta_r \tag{10}$$

$$C_B = 0.2877 + 0.0085\alpha + 0.0138\beta + 0.0019\delta_u - 0.0051\delta_r \tag{11}$$

For flight M-16

$$C_y = 0.6555 + 0.0144\alpha + 0.0256\beta + 0.0062\delta_u - 0.0154\delta_r \tag{12}$$

$$C_B = 0.2913 + 0.0074\alpha + 0.0130\beta + 0.0021\delta_u - 0.0058\delta_r \tag{13}$$

*In the flight-designation system used for the M2-F2, "M" refers to the vehicle, and the following digits designate the flight number.

The results are shown more clearly in figures 5 and 6 in which time histories of the maneuvers are presented with calculated components of equations (10) and (12). Data from flight M-10 are presented in figure 5 and from flight M-16 in figure 6. Also shown are the variations of spanwise centers of pressure, which were calculated from the relationship between the bending-moment and the shear coefficients. This relationship is

$$Z_{cp} = \frac{C_B}{C_y} \tag{14}$$

As shown in table II, the probable errors of the data fit for flight M-16 are lower than for flight M-10. This closer fit of the data is attributed to the higher dynamic pressure during the maneuver of flight M-16. However, the maneuvers were made at slightly different Mach numbers and the ranges of variables differed. The assumption of linear coefficients could also contribute to a poor data fit.

The components of the vertical-tail load coefficients (see figs. 5 and 6) that occurred during the relatively severe maneuvers analyzed indicate that most of the total vertical-tail load is due to the basic zero-condition load component C_{y_0}. The large magnitude of this component indicates that the flow is impinging on the vertical tail at a larger angle than might be expected. The variation of the sideslip load component $C_{y_\beta}\beta$ is fairly large and is a significant component in structural-design considerations. The angle-of-attack load component $C_{y_\alpha}\alpha$, too, is of significant magnitude. The rudder and upper-flap load components $-C_{y_{\delta_r}}\delta_r$ and $C_{y_{\delta_u}}\delta_u$ were also of significant magnitude; however, their variation results in tail loads of opposite direction, which tend to compensate for each other.

A rudder/upper-flap interconnect (referred to as a rudder-to-aileron interconnect in ref. 6) was incorporated into the M2-F2 control system primarily for control purposes. An adverse-yaw problem was anticipated; hence, the rudder was automatically deflected as aileron control was applied with the upper flaps. Figures 5 and 6 show that the rudder effect on the tail load is slightly larger than the upper-flap effect; thus, the rudder/upper-flap interconnect provided a favorable tail-load contribution to overcome any potential adverse-yaw problem. The flight data show that the interconnect results in an effect that tends to reduce the overall magnitude of the vertical-tail loads.

The total calculated load coefficients (eqs. (10) and (12)) compare favorably with the flight data (figs. 5 and 6). This comparison indicates that the flight-determined equations that define the load-component coefficients closely predict the actual load coefficient. The spanwise center of pressure for the two flights varies from 43 percent to 51 percent of the vertical-tail reference span b_t. The data from flight M-16, which are considered to be the most reliable, indicate that the center-of-pressure location varies from 43 percent to 47 percent of the reference span.

No plotted data of the bending-moment coefficient are presented because they are closely related to the normal-force coefficient through equation (14). The trends of the bending-moment data correspond closely to the normal-force-coefficient data in

figures 5 and 6. The bending-moment-component coefficients in table II show closer correlation between the values obtained for the two maneuvers than do the normal-force-component coefficients. The values for flight M-16, however, are still considered to be more reliable than those from flight M-10.

Control-Surface Hinge Moments

The flight-determined variations of control-surface hinge-moment coefficient with angle of attack and control-surface deflection are presented in figures 7 to 9 and compared with data obtained on the flight vehicle in the Ames 40- by 80-Foot Wind Tunnel. The test configurations and conditions for these tests are presented in reference 7.

Flight-measured upper-flap hinge-moment coefficients are compared in figure 7 with the wind-tunnel results. The rate of change of hinge-moment coefficients with upper-flap deflection (for constant angle of attack) is much less than the wind-tunnel predictions indicate. The flight data and the wind-tunnel data indicate that this rate of change (or slope) is reasonably linear (for constant angle of attack), although the slopes are significantly different in magnitude. No explanation of this discrepancy is available at this time.

Flight-measured lower-flap hinge-moment coefficients are compared in figure 8 with the wind-tunnel results. A sharp nonlinearity occurs in the wind-tunnel data between lower-flap deflections of 20° and 10°. The flight data do not agree closely in magnitude to the wind-tunnel data, but the rate of change (slope) of the coefficient with lower-flap deflection (for constant angle of attack) does compare favorably with the wind-tunnel data at lower-flap deflections of 20° or greater. The nonlinearity in the wind-tunnel data was not observed for the limited range of data obtained from flight tests.

Flight-measured rudder hinge-moment coefficients are compared in figure 9 with the wind-tunnel results. The rate of change of coefficient between 5° and 10° of rudder deflection shows agreement between flight data and wind-tunnel predictions. The overall range of data investigated in flight indicates some nonlinearity of hinge-moment coefficient associated with rudder deflection. The magnitudes of coefficients of the flight data agree closely with the wind-tunnel results.

Since insufficient information is available on the nature of the flow occurring near the control surfaces during the wind-tunnel tests and the flight tests, an explanation of the discrepancies between the flight data and the wind-tunnel data would be conjecture. Consequently, only the primary differences between the wind-tunnel test conditions and the flight test conditions are presented. These differences were:

1. The wind-tunnel tests were conducted at Reynolds numbers from 1.53×10^6 to 1.66×10^6 per foot (5.02×10^6 to 5.44×10^6 per meter). The flight Reynolds numbers were from 1.94×10^6 to 2.46×10^6 per foot (6.38×10^6 to 8.07×10^6 per meter).

2. Wind-tunnel mounts were used to support the M2-F2 vehicle during the wind-tunnel tests. The mounts may have created flow patterns unlike those existing in flight (see ref. 7).

3. The wind-tunnel tests were conducted at a steady-state Mach number of approximately 0.25, whereas the flight tests were conducted at varying Mach numbers from approximately 0.42 to 0.62.

4. The wind-tunnel tests were conducted at a free-stream dynamic pressure of 85 lb/ft^2 (4080 N/m^2), and the flight tests were conducted at free-stream dynamic pressures of 200 lb/ft^2 (9576 N/m^2) or higher.

Considering the overall correlation of wind-tunnel hinge-moment data with flight data, it is suggested that designers of lifting-body configurations be conservative in sizing control-surface structures and control-surface drive systems.

CONCLUDING REMARKS

Low-speed aerodynamic-loads data were obtained in flight tests of the M2-F2 lifting-body vehicle. The general subsonic load characteristics of the M2-F2 vertical tail were determined with sufficient accuracy to provide structural designers with usable full-scale flight data for comparative purposes. In addition, a comparison of the flight-determined control-surface hinge-moment data with wind-tunnel predictions provides an insight into the structural design of other lifting-body-type aircraft.

Large inward tail-load coefficients occurred on the vertical tail at zero aircraft attitude and control-surface position. The right vertical-tail-load coefficient increased with (1) increasing positive angle of attack, (2) increasing positive angle of sideslip, (3) increasing rudder deflection, and (4) decreasing upper-flap deflection.

The increase in vertical-tail loads due to rudder deflection was generally of the same magnitude as the decrease in vertical-tail loads resulting from upper-flap deflection, i.e., during interconnected rudder and upper-flap condition, little net change in the magnitude of tail loads was observed.

The vertical-tail spanwise center of pressure was determined to be approximately 45 percent of the vertical-tail reference span.

Significant differences between wind-tunnel-measured and flight-measured upper-flap hinge-moment coefficients and lower-flap hinge-moment coefficients were found. However, insufficient information was available to identify the source of the discrepancies. Flight-measured rudder hinge-moment coefficients compared well with wind-tunnel predictions.

Considering the overall results of the flight loads measurements on the M2-F2 lifting body, it is suggested that designers approach the prediction of lifting and control-surface aerodynamic loads on this type of vehicle with conservatism until more specific information becomes available.

Flight Research Center,
National Aeronautics and Space Administration,
Edwards, Calif., August 9, 1968,
727-00-00-01-24.

REFERENCES

1. Dennis, David H.; and Edwards, George G.: The Aerodynamic Characteristics of Some Lifting Bodies. NASA TM X-376, 1960.

2. Kenyon, George C.; and Edwards, George G.: A Preliminary Investigation of Modified Blunt 13° Half-Cone Re-Entry Configurations at Subsonic Speeds. NASA TM X-501, 1961.

3. Rakich, John V.: Aerodynamic Performance and Static-Stability Characteristics of a Blunt-Nosed, Boattailed, 13° Half-Cone at Mach Numbers From 0.6 to 5.0. NASA TM X-570, 1961.

4. Kenyon, George C.; and Sutton, Fred B.: The Longitudinal Aerodynamic Characteristics of a Re-entry Configuration Based on a Blunt 13° Half-Cone at Mach Numbers to 0.92. NASA TM X-571, 1961.

5. Pyle, Jon S.; and Swanson, Robert H.: Lift and Drag Characteristics of the M2-F2 Lifting Body During Subsonic Gliding Flight. NASA TM X-1431, 1967.

6. Holleman, Euclid C.: Stability and Control Characteristics of the M2-F2 Lifting Body Measured During 16 Glide Flights. NASA TM X-1593, 1968.

7. Mort, Kenneth; and Gamse, Berl: Full-Scale Wind-Tunnel Investigation of the Aerodynamic Characteristics of the M2-F2 Lifting-Body Flight Vehicle. NASA TM X-1588, 1968.

8. Skopinski, T. H.; Aiken, William S. Jr.; and Huston, Wilber B.: Calibration of Strain-Gage Installations in Aircraft Structures for the Measurement of Flight Loads. NACA Rept. 1178, 1954.

TABLE I. – PHYSICAL CHARACTERISTICS OF THE M2-F2 VEHICLE

Body –	
Planform area, feet^2 (meters^2):	
Actual	160 (14.9)
Reference	139 (12.9)
Longitudinal length, feet (meters):	
Actual	22.2 (6.76)
Reference	20.0 (6.11)
Span, without rudder flare, feet (meters):	
Actual	9.63 (2.94)
Reference	9.54 (2.91)
Aspect ratio, based on reference dimensions	0.655
Body leading-edge sweep, degrees	77
Lower flap –	
Area, feet^2 (meters^2)	15.23 (1.41)
Span, feet (meters)	5.42 (1.65)
Chord, feet (meters)	2.81 (0.86)
Deflection, degrees:	
Pilot's control authority, down	5 to 30
Pitch stability augmentation system authority	±5
Upper flaps, two –	
Area, each, feet^2 (meters^2)	9.57 (0.89)
Span, each, feet (meters)	4.28 (1.31)
Chord, feet (meters)	2.23 (0.68)
Deflection, each flap, degrees:	
Pitch trim (symmetric travel), up	0 to 35
Pilot's aileron authority (asymmetric travel)	±5
Roll stability augmentation system authority (asymmetric travel)	±2.5
Vertical stabilizers, two –	
Area, each, feet^2 (meters^2)	16.10 (1.50)
Exposed panel area S_t (reference area for loads), feet^2 (meters^2)	13.65 (1.268)
Exposed panel span b_t (reference span for loads), feet (meters)	2.70 (0.823)
Height, trailing edge, feet (meters)	3.79 (1.16)
Chord, feet (meters):	
Root	7.36 (2.24)
Tip	2.58 (0.79)
Leading-edge sweep, degrees	62.3
Rudders, two –	
Area, each, feet^2 (meters^2)	5.27 (0.49)
Span, each, feet (meters)	4.20 (1.28)
Chord, feet (meters)	1.25 (0.38)
Deflection, degrees:	
Pilot's effective control authority	12
Yaw stability augmentation system authority	4.2
Weight, including pilot, pounds (kilograms)	6000 (2722)
Center of gravity:	
Percentage of actual length	49
Percentage of reference length	54

TABLE II. – RESULTS OF ANALYSIS OF VERTICAL-TAIL FLIGHT LOAD-COMPONENT COEFFICIENTS

	C_{y_0}	C_{y_α}	C_{y_β}	$C_{y_{\delta_u}}$	$C_{y_{\delta_r}}$	C_{B_0}	C_{B_α}	C_{B_β}	$C_{B_{\delta_u}}$	$C_{B_{\delta_r}}$
Flight M-10, q = 225 to 260 lb/ft^2 (10,773 to 12,449 N/m^2), M = 0.59 to 0.62, α = -3.8° to 7.6°, β = -3.7° to 4.6°, δ_r = 0.3° to -10.5°, δ_u = -3.2° to -18.6°										
Coefficient	0.6009	0.0221	0.0324	0.0038	0.0109	0.2877	0.0085	0.0138	0.0019	0.0051
Probable error of coefficient	.0098	.0011	.0021	.0017	.0028	.0044	.0005	.0010	.0008	.0013
Percent probable error of coefficient	1.6	4.8	6.6	43.9	25.8	1.5	5.6	7.0	40.8	25.1
Flight M-16, q = 260 to 296 lb/ft^2 (12,449 to 14,172 N/m^2), M = 0.46 to 0.49, α = -3.6° to 4.0°, β = -4.2° to 4.0°, δ_r = 0.1° to -12.5°, δ_u = -6.3° to -22.5°										
Coefficient	0.6555	0.0144	0.0256	0.0062	0.0154	0.2913	0.0074	0.0130	0.0021	0.0058
Probable error of coefficient	.0074	.0006	.0018	.0008	.0010	.0044	.0004	.0011	.0005	.0006
Percent probable error of coefficient	1.1	4.2	7.3	12.3	6.8	1.5	4.8	8.5	21.5	10.6

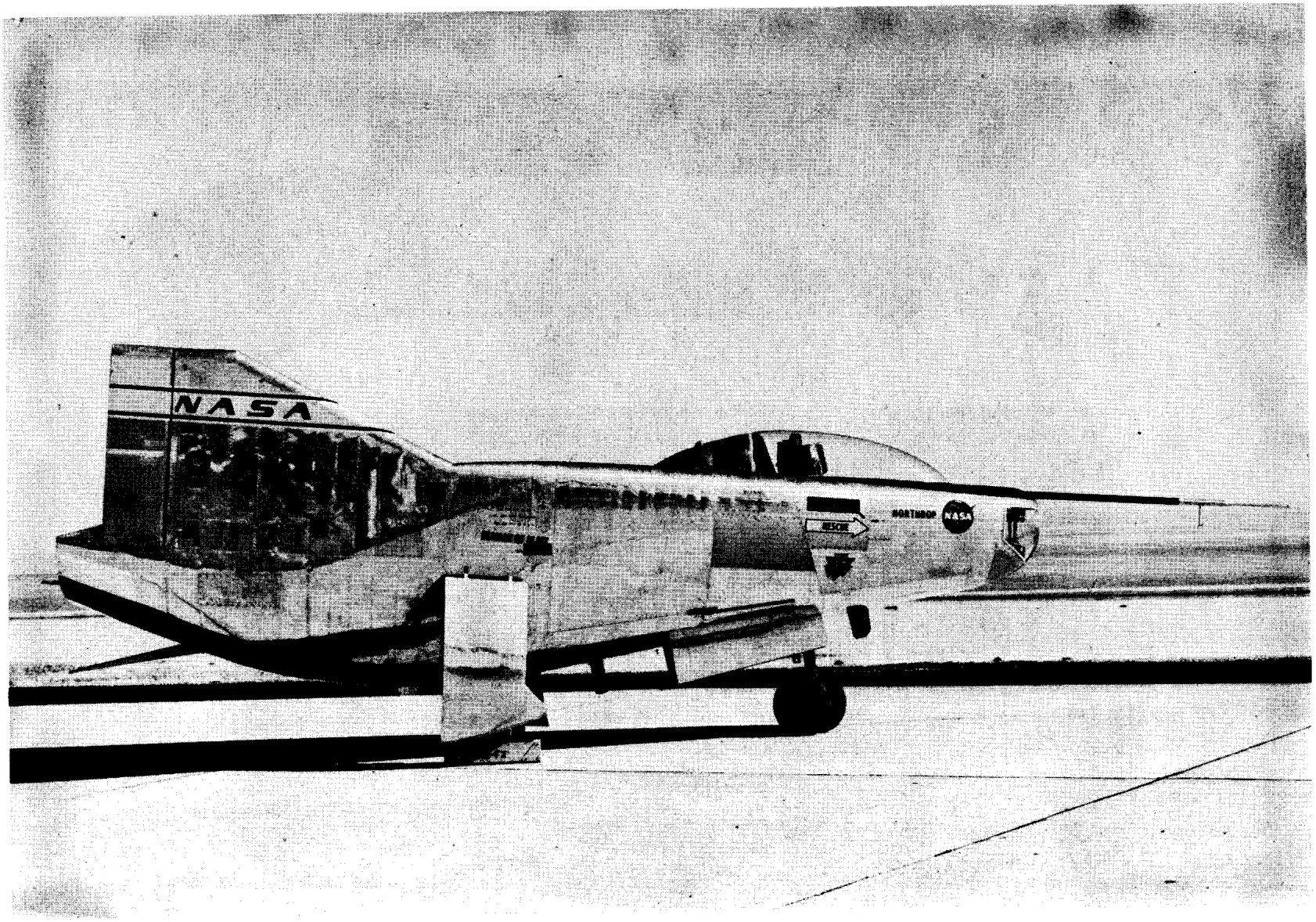

(a) Side view.

E-14333

Figure 1.– Photos of M2-F2 vehicle.

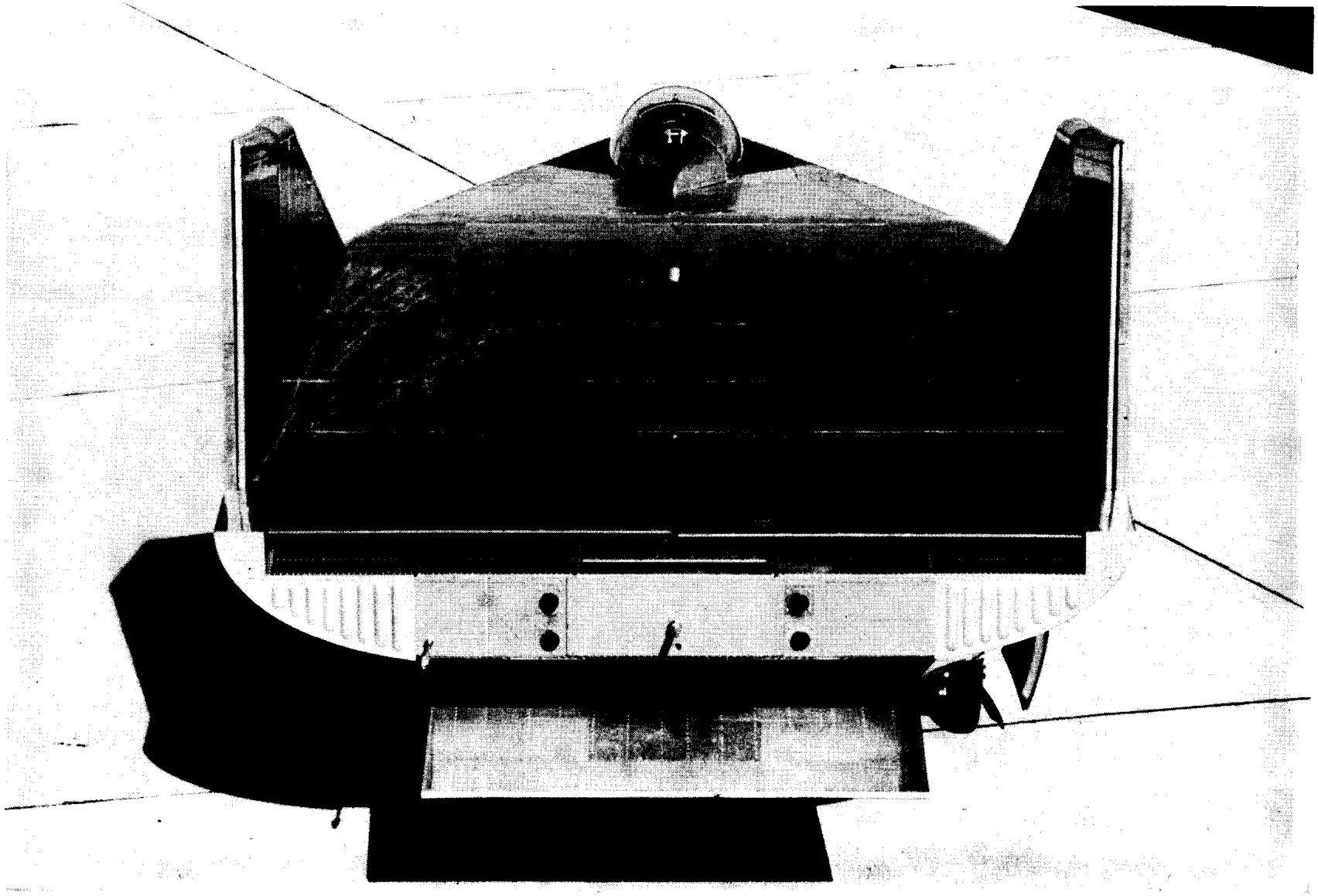

(b) Rear view (0° rudder flare).

E-14350

Figure 1. – Concluded.

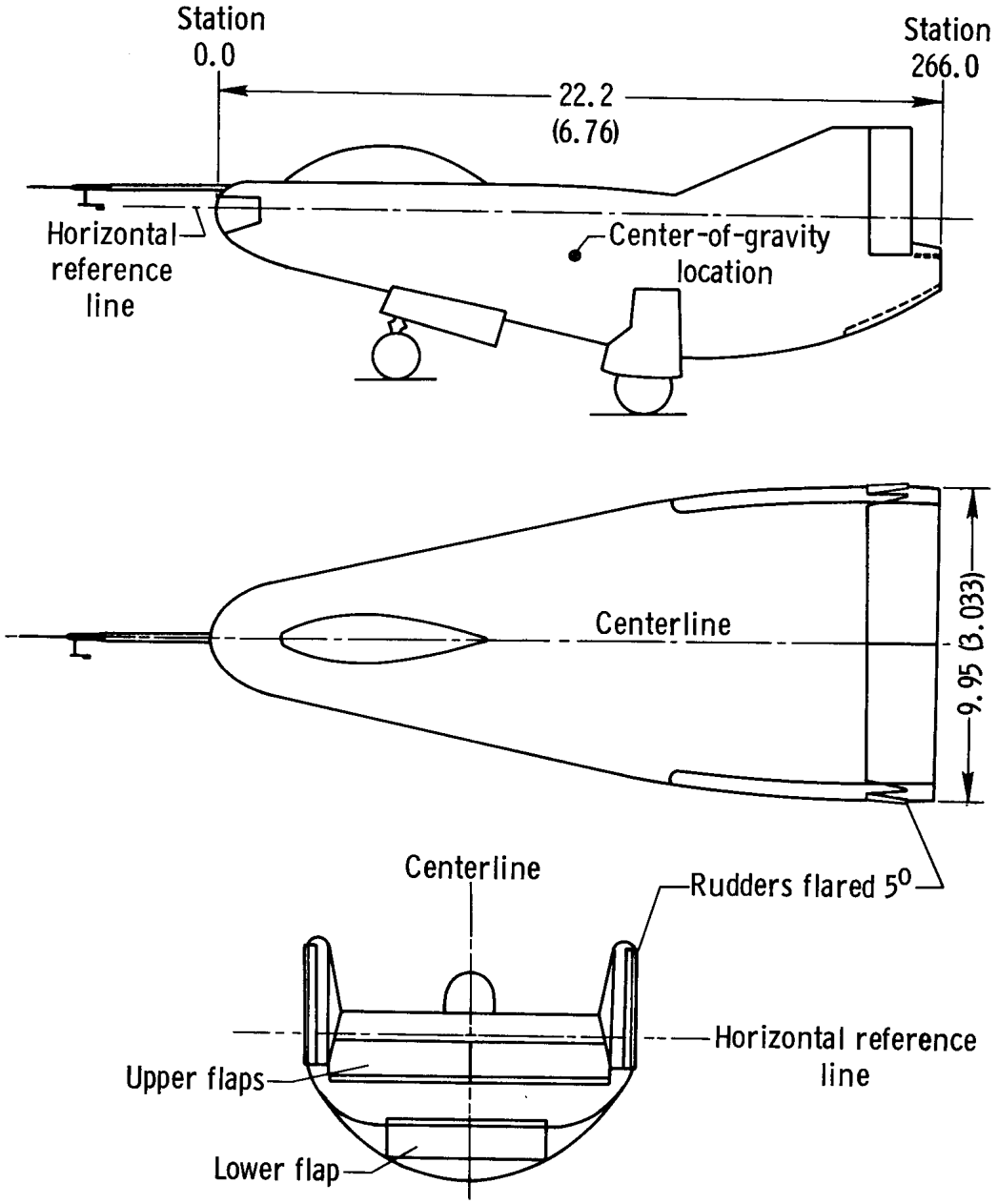

Figure 2. – **Three-view drawing** of the M2-F2 aircraft. **Dimensions in feet** (meters).

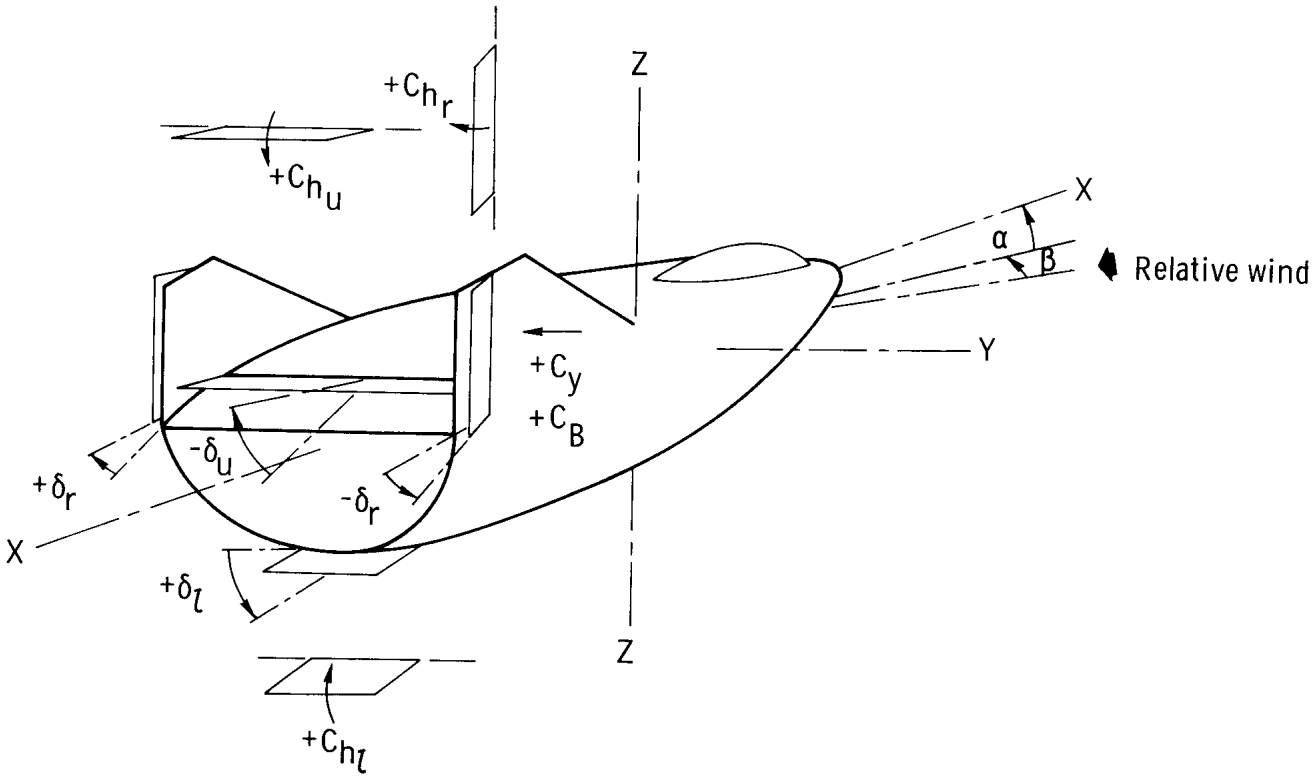

Figure 3. – Sign convention for the M2-F2 aircraft.

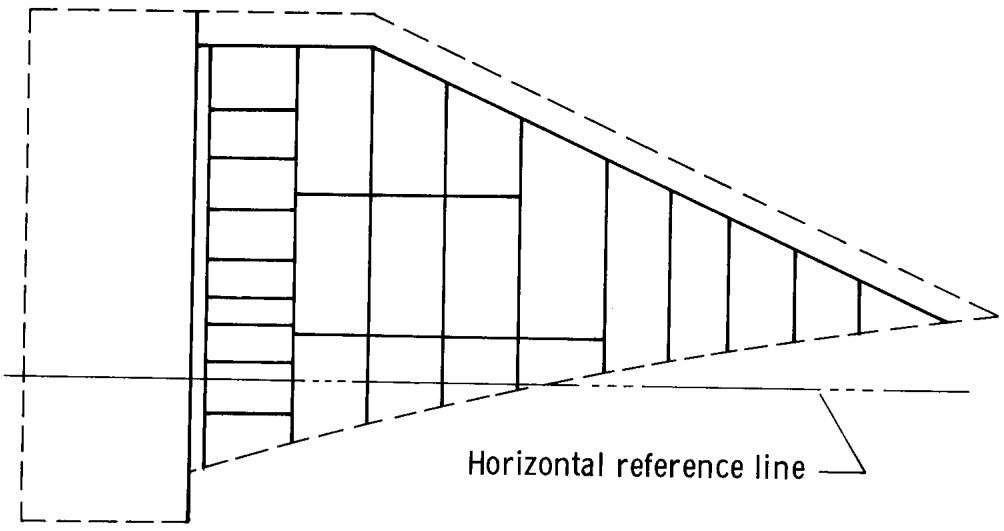

Figure 4. – M2-F2 vertical-tail substructure.

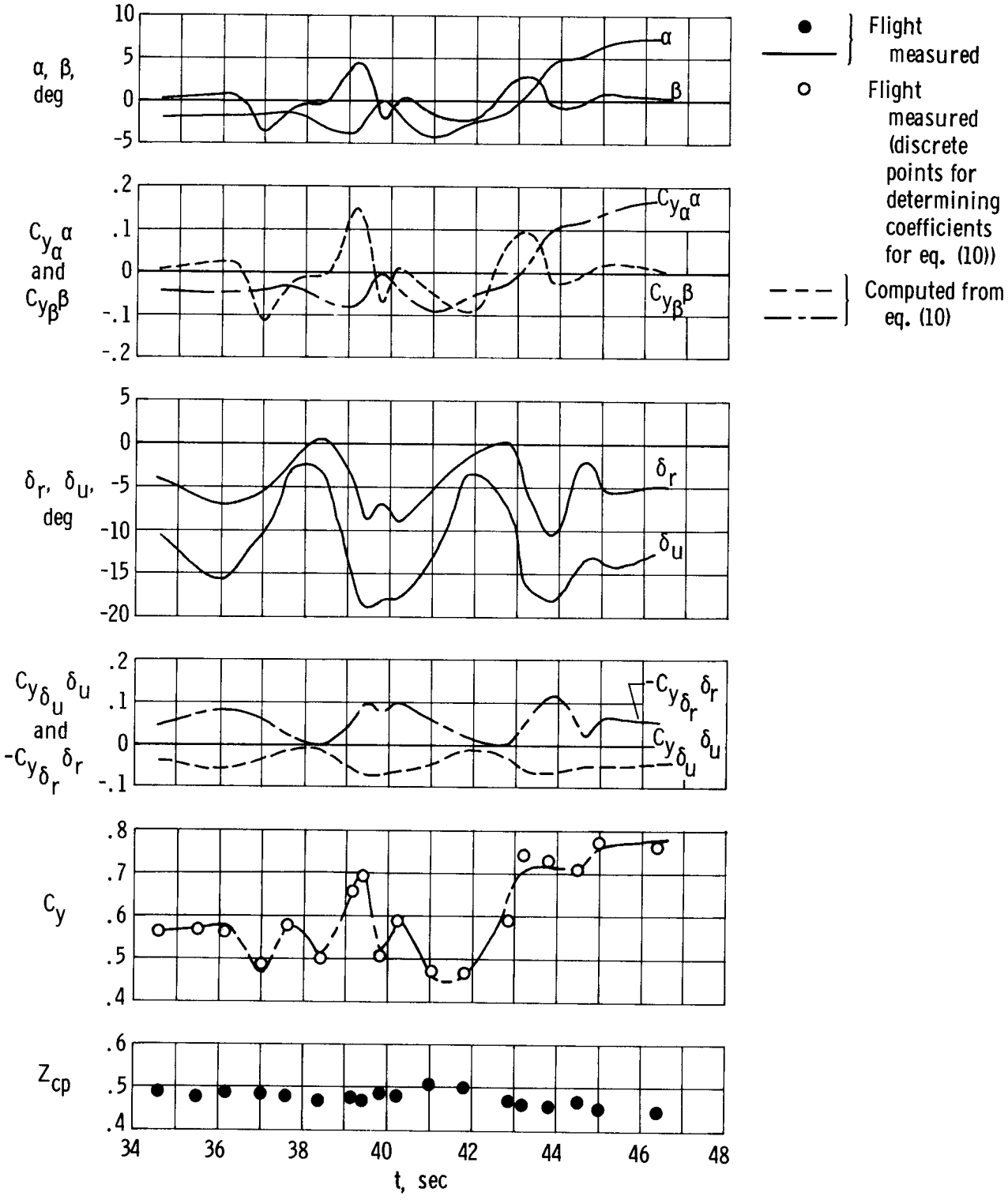

Figure 5. – Time history of flight M-10 maneuver. q = 225 to 260 lb/ft^2 (10,773 to 12,449 N/m^2); M = 0.59 to 0.62.

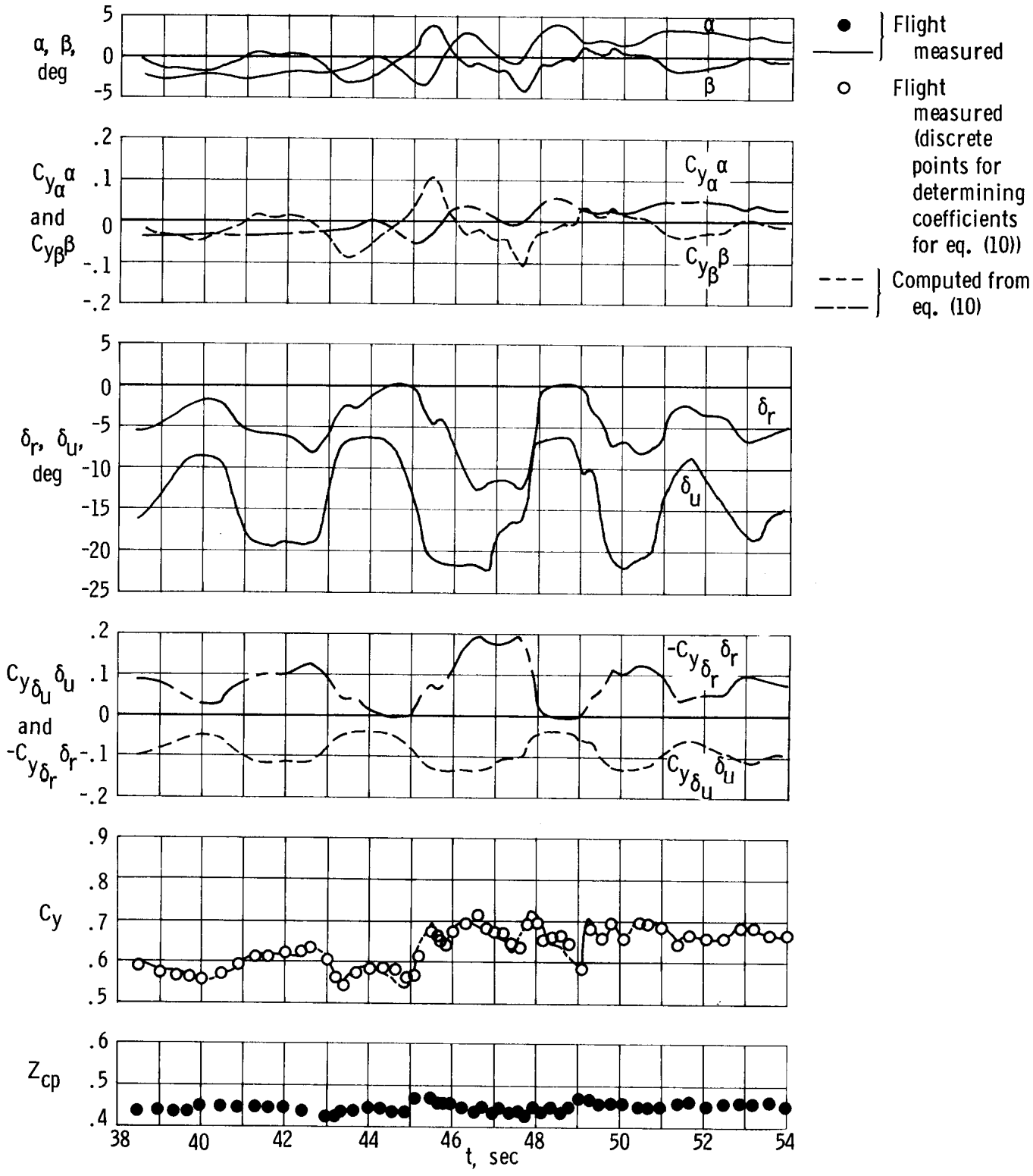

Figure 6. – **Time history of flight** M-16 maneuver. q = 260 to 296 lb/ft^2 (12,449 to 14,172 N/m^2); M = 0.46 to 0.49.

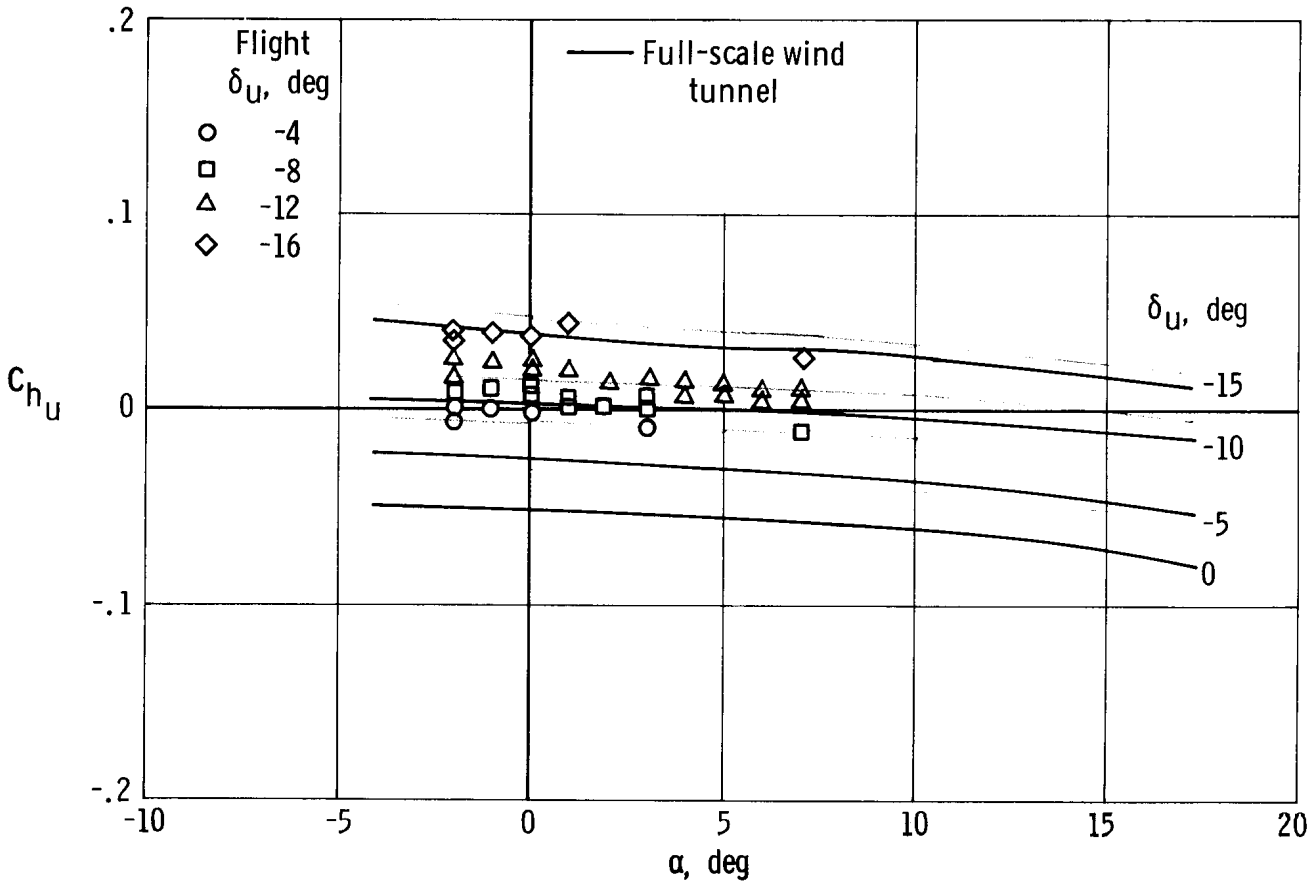

Figure 7. – Comparison of flight-measured upper-flap hinge-moment coefficients with full-scale wind-tunnel predictions.

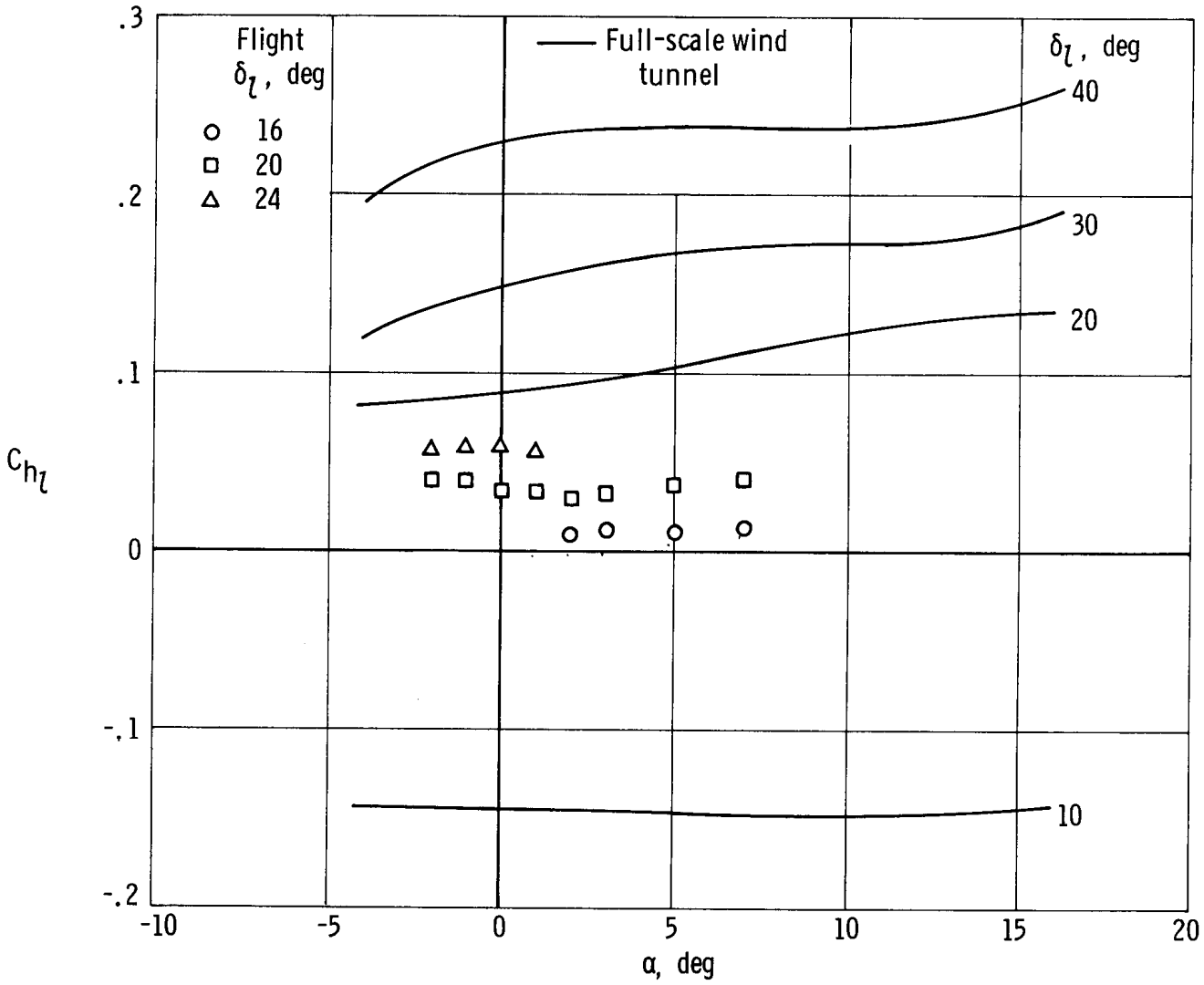

Figure 8. – Comparison of flight-measured lower-flap hinge-moment coefficients with full-scale wind-tunnel predictions.

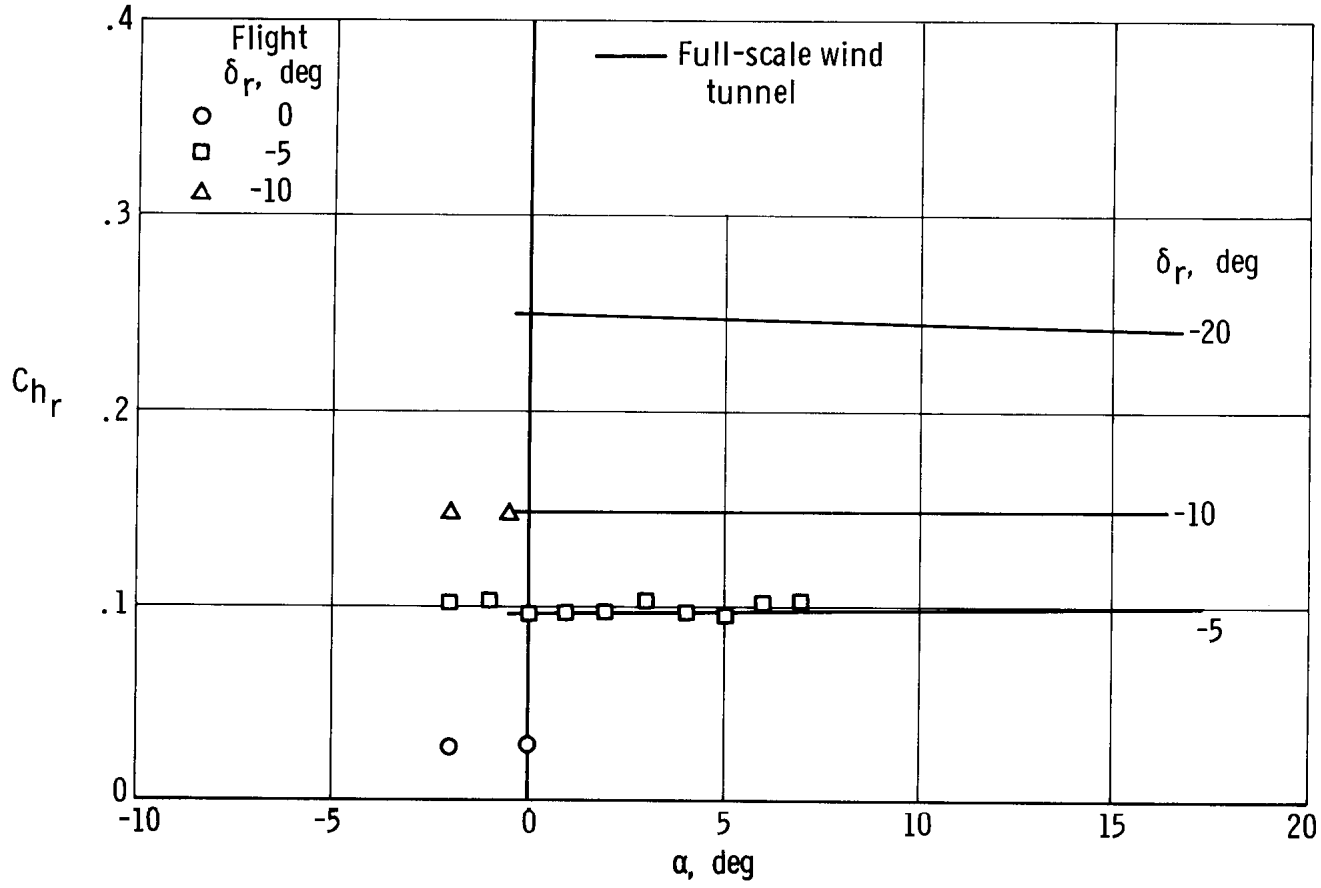

Figure 9. – Comparison of flight-measured rudder hinge-moment coefficients with full-scale wind-tunnel predictions.